Appl. Phys. A 73, 547–554 (2001) / Digital Object Identifier (DOI) 10.1007/s003390100947

Applied Physics A
Materials
Science & Processing

Deposition of mass-selected cluster ions using a pulsed arc cluster-ion source

B. Klipp, M. Grass, J. Müller, D. Stolcic, U. Lutz, G. Ganteför*, T. Schlenker, J. Boneberg, P. Leiderer

Fachbereich Physik, Universität Konstanz, 78457 Konstanz, Germany

Received: 30 May 2001/Accepted: 14 June 2001/Published online: 2 October 2001 –

Abstract. A PACIS (pulsed arc cluster-ion source) developed for high average cluster-ion currents is presented. The performance of the PACIS at different operational modes is described, and the suitability for cluster-deposition experiments is discussed in comparison with other cluster-ion sources. Maximum currents of mass-selected cluster ions of 3–6 nA of small Si_n^- ($n = 4$–10) clusters and 0.3–0.5 nA of large $Al_n^{+/-}$ ($n = 20$–70) clusters are achieved. The mass-selected cluster ions are soft-landed on a substrate at residual kinetic energies lower than 1 eV/atom, and the samples are characterized by X-ray photoelectron spectroscopy and scanning tunneling microscopy. First results on the soft landing of "magic" Si_4^- clusters on graphite are presented.

PACS: 36.40.-c; 61.46.+w; 81.07.Nb

The preparation of nanostructures on surfaces is one of the major tasks in technology and basic research. Applications of nanostructured surfaces are abundant and cover a wide range from heterogeneous catalysis to high-density computer memories. From the point of view of basic research, many of the properties of small three-dimensional nanostructures and two-dimensional islands on surfaces are not well understood yet. For example, there is no systematic study of the size-dependence of the electronic structure of clusters of simple metals on surfaces, although free clusters of such metals show strong variations depending on the number of delocalized electrons [1]. Concerning the chemical properties, there are first results on the size-dependence of the catalytic properties of small clusters on inert substrates [2], but there are only very few systematic studies yet (see below). The kind of research focussing on the electronic and chemical properties of monodispersed small clusters on surfaces is only at its beginning. The reason is that it is difficult to deposit clusters with a perfectly monodispersed size distribution on a surface.

Another driving force for the study of clusters on surfaces is the search for new materials. Once it was possible to generate sufficient amounts of C_{60}, it turned out that these stable carbon clusters could be used as building blocks for new solids [3]. Stable clusters exist for many other materials than just carbon, and it might be possible to build new solids from them, too. However, in many cases these clusters are highly reactive with respect to oxygen or water and cannot be extracted and separated by the chemical methods used for fullerenes. Therefore, more general methods for generation of sufficient amounts of clusters of various materials and for mass separation and deposition are needed.

The deposition of mass-selected cluster ions which have been preformed in the gas phase is such a general method to prepare nanostructures of various materials on surfaces [4–25]. It has certain advantages compared to other techniques like electron beam lithography and the growth of islands from single atoms evaporated on a surface:

(i) the deposited clusters are mass-selected in a mass spectrometer prior to the deposition and the size distribution is truly monodispersed, corresponding to a well-defined number of atoms in the clusters.
(ii) the clusters generated in the gas phase presumably relax into their most stable geometric structure. Such clusters have geometric structures different from those of islands grown from deposited atoms or prepared using lithographic techniques. For example, C_{60} fullerenes will not be formed by lithographic structuring of graphite or by carbon-vapor deposition. The relaxed clusters are probably more suitable as building blocks for new cluster materials and have a more uniform geometric structure, i.e. they have more uniform chemical and electronic properties.

The mass separation prior to the deposition is usually achieved by electric or magnetic fields. Therefore, the clusters need to be charged, which limits this method to very small amounts of material and as a consequence this approach is thought of as a method just to identify clusters with promising properties. Once a cluster of a certain material and size is found, a different method for the generation of larger quantities must be developed (probably based on chemical techniques). As a rule of thumb, a cluster-ion source should

*Corresponding author.
(Fax: +49-7531/883091, E-mail: gerd.gantefoer@uni-konstanz.de)

generate more than 1 nA of a selected cluster size for small clusters ($n < 10$) and more than 0.1 nA for larger clusters ($10 < n < 100$) to conduct such types of experiments within a reasonable time.

The bottleneck of the method is the generation of sufficient intensities of cluster-ion beams. Here, one goal is to test a pulsed arc cluster-ion source (PACIS) [26–28] for its suitability for deposition experiments. This source has previously been used for such experiments [29], but no quantitative values for the obtained intensities have been given yet.

For the generation of cluster ions, a few different types of cluster sources are used. In early cluster-deposition experiments a liquid-metal ion source [4], a laser vaporization source [5] or sputter sources [6, 7] have been used. More recently, in most experiments a sputter source is used for the generation of positively or negatively charged Ag_n, Au_n, Pd_n and Pt_n clusters. For example, the deposition of Ag_n clusters on Pd [8] and Pt [9, 10] single-crystal surfaces has been studied at different deposition energies ($E_{dep} = 1$–20 eV per cluster atom). Using a similar experimental setup the evolution of the electronic structure of Pt_n and Pd_n clusters on Ag (110) has been studied by photoemission [11, 12]. In the last two years an improved version of the sputter source has been used to study the impact and the deposition of metal clusters on highly ordered pyrolytic graphite (HOPG) [13–19]; for the deposition of larger Ag_n clusters ($n = 50$–400) on HOPG a gas aggregation source is used [20–22]. Heiz et al. recently developed an improved laser vaporization source for the deposition of transition-metal clusters (Ni_n [23, 24], Pt_n [25]) on metal oxide surfaces with the goal to study systematically the size dependence of the catalytic properties of these clusters.

The different sources have certain advantages and disadvantages. In the gas aggregation source [30–32] the material is heated and a vapor pressure sufficient for the condensation of clusters must be achieved. Applications of this source are limited to materials with relatively low boiling points, excluding many interesting elements like carbon and silicon. Sputtering of solids by high-energy ions yields high intensities of small cluster ions for Ag, Al, Au, Pt and C (for the most recent description see [33]: C_4^-: 46 nA, Al_4^-: 23 nA, Al_4^-: 2 nA). However, for clusters larger than $n = 10$ the intensities drop dramatically ([33]: C_{10}^-: 400 pA, Al_{10}^-: 40 pA, Al_{10}^-: 100 pA). The most common source in gas phase cluster research is the laser vaporization source [34, 35], in which the material is vaporized using a high-energy laser pulse. Previously, the achieved cluster-ion currents using this source [5] were very small (< 50 pA). Recently however Heiz et al. have developed an improved laser vaporization source [36], which produces cluster-ion currents of about 1 nA for Nb_n clusters with $n = 10$–20 atoms.

The PACIS [26–28] is basically similar to the laser vaporization source, but the material is vaporized by a pulsed electric arc. It was first developed as a pulsed cluster-ion source for laser spectroscopy experiments on free clusters [26]. In principle, the amount of material vaporized in each pulse depends solely on the power of the pulsed arc. The cluster intensity can be optimized by increasing the repetition rate and the pulse power and is limited by the maximum thermal load in the source and the gas load of the vacuum system. At low repetition rates (10–50 Hz) cluster-ion intensities comparable or higher than the ones obtained using a laser vaporization source have been achieved [34]. The application of the source is limited to conducting materials (e.g. Ag [37], C [38], Si [39], Pb [40]). However, it can also be used to generate clusters of non-conducting materials with low melting points (S_n [41], P_n [42]). A PACIS has already been used for cluster deposition [29]. However, the cluster-ion currents which can be achieved using a PACIS are not known yet.

Here, we describe a PACIS optimized for the generation of high cluster-ion currents. The source is operated at high repetition rates (300–1000 Hz), and the amount of material vaporized in each single shot is optimized. With our experimental setup, currents of monodispersed cluster ions of 3–6 nA for small Si_n^- ($n = 4$–10) clusters and of 0.3–0.5 nA for large Al_n^+ ($n = 20$–70) clusters can be achieved. The cluster ions are mass-selected in a 45°-sector magnet and guided into an ultra high vacuum (UHV) chamber. There, the ions are soft-landed on a sample with residual kinetic energies lower than 1 eV/atom. The samples are characterized in situ using X-ray photoelectron spectroscopy (XPS) and can be transferred to a scanning tunneling microscope (STM) operated under UHV.

First results on the deposition of Si_4 clusters are presented. 'Magic' silicon clusters like Si_4, Si_7 and Si_{10} might be suitable as building blocks for new cluster materials, if they do not merge forming larger particles. Therefore, we deposited Si_4^- clusters on an inert surface (HOPG) at room temperature. The clusters diffuse on the surface and might form larger aggregates of bulk silicon or islands consisting of weakly interacting Si_4 clusters. We studied the surfaces using XPS and scanning tunneling microscopy and found some indications that the clusters do not merge but behave like weakly bound molecules adsorbed on the surface.

1 Experimental setup

A sketch of the experimental setup is shown in Fig. 1. It can be separated into six parts (1.1 cluster source, 1.2 ion extraction, 1.3 mass separation, 1.4 soft landing, 1.5 photoelectron spectroscopy and 1.6 scanning tunneling microscopy), which will be discussed in the following.

1.1 Cluster source

Figure 2 displays a schematic of the cluster-ion source. A former version of this source suitable for operation at low repetition rates (< 50 Hz) is described in [28]. In the source a pulsed electric arc burns within the center of a small cube ($\sim 4 \times 4 \times 4\,cm^3$) manufactured from boron nitride. The cube has two channels perpendicularly intersecting each other in the center. The electrodes are inserted from opposite sides into the larger bore (cathode: diameter 13 mm, anode: diameter 5 mm) and face each other at the center of the cube leaving a gap of about 1 mm. A carrier gas pulse (usually helium) produced by pulsed valves (solenoid valve (General Valve)) flows through the second channel and the gap between the electrodes. The carrier gas leaves the ceramic cube on the opposite side, streaming into the extender. Simultaneously with the gas pulse the dc electric arc is ignited, leading to the vaporization of material from the cathode. The metal vapor and the helium mix within the discharge and the resulting plasma is flushed into the extender. Depending on the kind

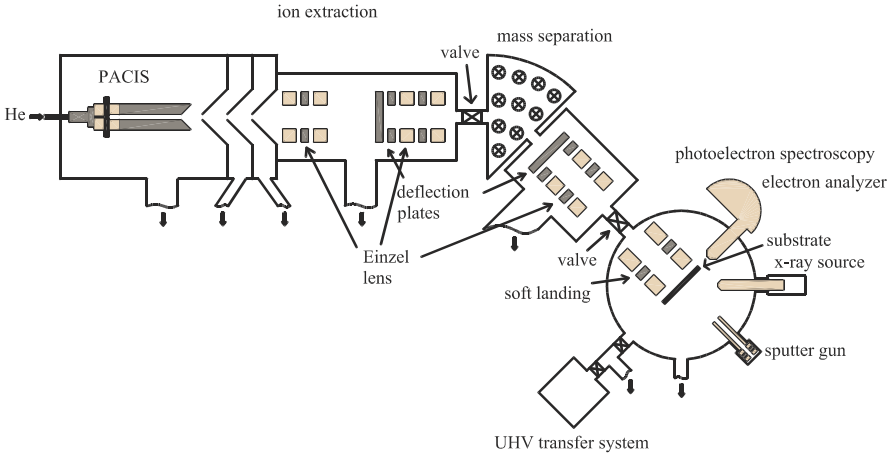

Fig. 1. Experimental setup. The clusters are generated with a pulsed arc cluster-ion source (PACIS), extracted from the supersonic jet after passing three differential pumping stages and accelerated up to a kinetic energy of 500–1500 eV. The ions are mass-separated in a 45°-sector magnet, guided into an ultra-high vacuum (UHV) chamber and soft-landed on a substrate. The sample can be characterized in situ using XPS. In addition, it can be transferred to a STM operated under UHV (not shown)

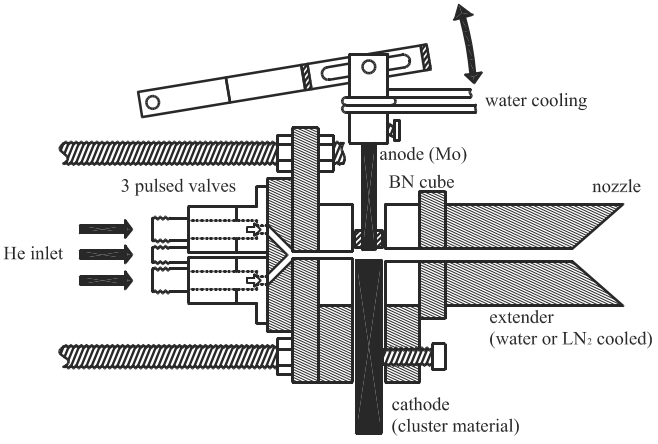

Fig. 2. Sketch of the pulsed arc cluster-ion source. The cathode is eroded by a pulsed electric arc burning in the ~ 1 mm gap between the two electrodes. The gap can be adjusted by moving the anode, which is manufactured from molybdenum. All metal parts are water-cooled. The three pulsed valves are operated alternatingly to achieve a maximum frequency of 1000 Hz. The length and the diameter of the extender can be changed to optimize the source for the generation of larger or smaller clusters

of clusters to be produced, a different design of the extender has to be chosen. For small Si_n^- clusters ($n = 4$–10) a short (50 mm) extender with a diameter of 5 mm is used. For larger Al_n^- clusters ($n = 10$–70) the extender is 200 mm long with a diameter of 3 mm. Finally, the clusters embedded in the carrier gas leave the source through a conical nozzle, forming a supersonic expansion. The conical nozzle has an opening angle of 30° and a length of 30 mm.

The source produces both positive and negative ions. For an optimum yield of ions both the ion intensity per cycle and the repetition rate have to be optimized. We found an optimum ion intensity per cycle for the following conditions:

– A "burning" voltage of the pulsed electric arc of about 80–120 V. At significantly higher voltages the ion yield decreases. Since the arc does not ignite at low voltage, in each cycle an additional high voltage (680 V)/low current (3 A) electric pulse is superimposed on the low voltage/high current (max. 2500 A) "burning" pulse. A simplified sketch of the power supply is shown in Fig. 3. The high-current burning pulse is produced by 100 transistors, and the "ignition" pulse generated using two high-voltage transistors is superimposed on the burning pulse.
– An intense He-gas pulse is crucial. To minimize the He-gas load in the vacuum system the gas pulse should be as short as possible. On the other hand, a strong flow is necessary for a high ion yield, probably because of neutralization dominating at low gas flow. We found an optimum ion intensity using an electromagnetic valve (General Valve). Such a valve can be operated up to a frequency of 350 Hz.

To achieve a repetition rate of up to 1000 Hz the following improvements have been made:

– The source body and the extender are water-cooled and the center cube is mounted in a water-cooled copper housing.
– Three pulsed valves work in an alternating mode, so that each valve operates at 333 Hz, resulting in a repetition rate of 1000 Hz (Fig. 2). The three valves are mounted as close as possible to the center cube to minimize the volume which has to be flooded with the carrier gas in each

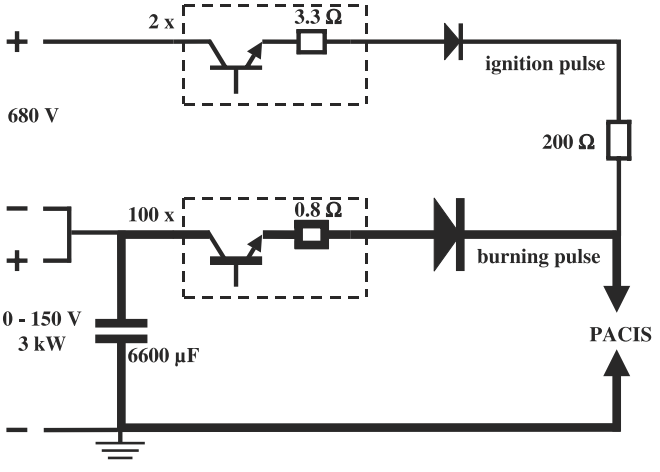

Fig. 3. The main electrical circuits of the pulsed power supply of the PACIS. The burning pulse is delivered from a capacitor charged to an adjustable voltage of 0–150 V and switched by 100 power-MOSFETs (metal oxide semiconductor field-effect transistors), each switching a current of about 25 A. The ignition pulse of 680 V and 3 A is added to the "burning" pulse. As soon as the arc ignites, the voltage between the two electrodes of the PACIS decreases to approximately the voltage of the main capacitor

pulse. Otherwise the gas flow through the gap between the electrodes decreases, reducing the ion intensity. The three outlets of the valves meet at the entrance channel of the cube.

1.2 Ion extraction

The source and the sample are set to ground potential. The ions are accelerated to a kinetic energy of 500–1500 eV, and the ion beam is guided through a metal shield kept at the corresponding potential (±500–1500 V for negatively/positively charged clusters). The advantage of this design is that the source is operated at ground potential and problems with discharges due to the low gas pressure in the source chamber are avoided.

One major problem at high repetition rates is the He-gas load. The pressure in the ion-extraction chamber has to be kept below 3×10^{-5} mbar. Otherwise the ion signal decreases due to inelastic scattering processes of the cluster ions with atoms of the residual gas. However, the openings of the skimmers of the three differential pumping stages (Fig. 1) cannot be too small and the distances between the three skimmers cannot be too large. Otherwise the ion signal decreases.

The third skimmer is set to an attractive potential of roughly 200 V. The preaccelerated ions enter the main acceleration chamber and are accelerated up to the maximum kinetic energy of 500–1500 V. An Einzel lens forms a well-defined cluster-ion beam, which is subsequently focussed by a second Einzel lens onto the entrance aperture of a 45°-sector magnet.

1.3 Mass separation

Mass separation is achieved by deflection in a magnetic field. The maximum field strength of the deflection magnet is 1 T, corresponding to a maximum mass of 1900 amu of the deflected ions at a kinetic energy of 1000 eV. Therefore, singly charged Al clusters up to a cluster size of 70 atoms can be deflected. For the experiments described here, the entrance aperture of the sector magnet is set to diameters of 15 mm and 8 mm, resulting in a mass resolution of $m/\Delta m = 10$ and 20, respectively. An example of a mass spectrum of small Si_n^- clusters with $n = 3$–8 is displayed in Fig. 4.

So far, we have determined cluster-ion intensities for two different sorts of clusters, aluminum and silicon clusters. The currents obtained at different operational conditions of the source are given in Table 1. For small clusters with $n < 10$ the PACIS gives smaller intensities than the sputter source [33]. However, for larger clusters with $n > 10$ the intensities are higher by an order of magnitude. Compared to the laser vaporization source described by Heiz et al. [36] the intensities are similar or slightly lower.

1.4 Soft-landing ion optics

After passing the magnet the ion beam is focussed by a third Einzel lens into the UHV chamber. In a small gap between the sample surface and the guiding tube of the ion beam the ions are decelerated in a homogenous electrostatic field. The potential of the sample can be varied by ±100 V with respect to ground potential. The amount of deposited cluster ions is determined by measuring the ion current using the sample as a Faraday cup.

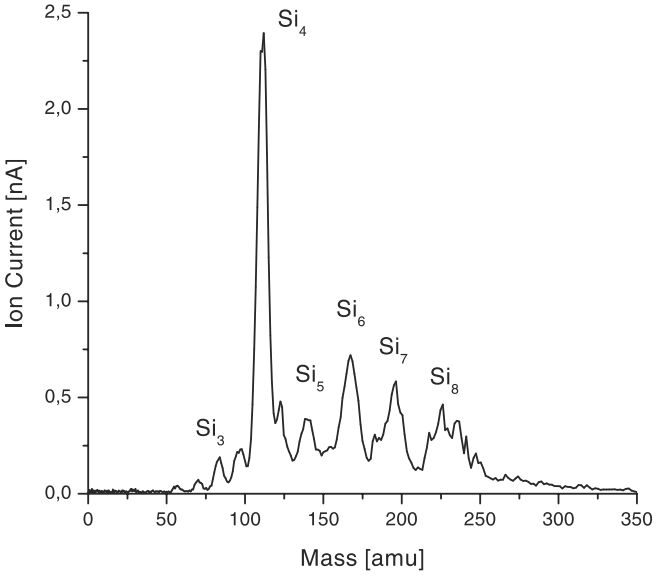

Fig. 4. Mass spectrum of Si_n^- cluster anions recorded at a repetition rate of 300 Hz using a short extender (length 50 mm, diameter 5 mm) and with a mass resolution of $m/\Delta m = 20$. The source is optimized for a maximum current of the "magic" cluster Si_4^-, and an intensity of about 2.4 nA is achieved at this resolution and at a residual kinetic energy of 0.75 eV/atom. For $n = 3$, 4, reactions with boron nitride yield small additional mass peaks

Table 1. Maximum cluster-ion currents obtained for various cluster sizes, extender geometries and repetition rates. All values are given for low mass resolution ($m/\Delta m = 10$)

Ion	Current	Extender	Repetition rate
Si_1^+	40 nA	Short	500 Hz
Si_4^-	6.5 nA	Short	300 Hz
Si_7^-	3 nA	Short	300 Hz
Si_{10}^-	1.5 nA	Short	300 Hz
Si_{20}^-	0.4 nA	Long	300 Hz
Si_{30}^-	0.3 nA	Long	300 Hz
Al_1^+	300 nA	Long	1000 Hz
Al_{13}^-	4 nA	Long	800 Hz
Al_{20}^-	3.5 nA	Long	800 Hz
Al_{40}^-	1 nA	Long	600 Hz
Al_{70}^-	0.5 nA	Long	600 Hz

To avoid fragmentation, the cluster ions should be decelerated to a minimum kinetic energy (E_{dep}). However, the kinetic energy of the cluster ions exhibits a certain width, and the deceleration to values lower than this causes a considerable loss of intensity: ions with slightly lower kinetic energy do not hit the sample surface any more, but turn around before reaching it. Therefore, the distribution of kinetic energies of the cluster ions should be as narrow as possible and it depends on the design of the ion extraction.

The width of the kinetic energy distribution can be measured by monitoring the ion intensity at the sample while scanning the sample potential. The derivative of the ion intensity gives the energy distribution. Figure 5 displays the widths (full width at half maximum: FWHM) obtained for three dif-

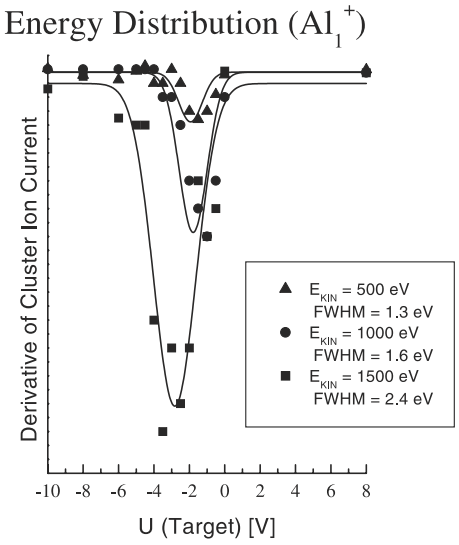

Fig. 5. Widths (full width at half maximum: FWHM) of the kinetic energy distributions of Al_1^+ ions corresponding to the derivative of the ion intensity measured at the sample while changing the sample potential. The widths depend on the kinetic energy of the ions ($E_{kin} = 500$ eV, 1000 eV and 1500 eV) and correspond to the minimum residual kinetic energy (E_{dep}) for soft landing of the ions

ferent kinetic energies (500 eV, 1000 eV, 1500 eV) for Al_1^+ ions. The widths range from 1.3 eV to 2.4 eV and are comparable to the corresponding values for experimental setups using a sputter source ([8–10]: 20 eV for Ag_7^+ clusters, [13]: 0.92 eV for Ag_4^+ clusters) or a laser vaporization source ([36]: 0.5 eV for Nb_1^+ ions). Therefore, for clusters larger than the trimer the residual kinetic energy is less than 1 eV/atom as required.

1.5 Photoelectron spectroscopy

The UHV chamber is equipped with an X-ray gun (Vacuum Generators XR3E2) and a hemispherical electron-energy analyzer (Omicron EA125 U5). With X-ray photoelectron spectroscopy the chemical composition of the sample surface can be monitored. The deposition of clusters takes about 1 h, and during this time not only cluster ions but also some neutral molecules may adsorb on the sample surface. With XPS, contamination such as oxygen or a hydrocarbon is detected and the amount of clusters deposited on the sample is measured. In addition, from the chemical shift of the XPS features it can be determined whether the clusters are pure or contaminated. For very small clusters ($n < 10$) there is a size-dependent line shift of the XPS peaks, which can be used to detect fragmentation or agglomeration of the deposited clusters [14, 15].

As a first example, Fig. 6 displays a comparison of XPS spectra of a clean HOPG surface with a HOPG surface covered with 2% of an atomic monolayer of Al_n clusters with $n = 70 \pm 3$. This corresponds to a charge of 0.025 nA h/cm^2. The clusters have been deposited with a residual kinetic energy of $E_{dep} = 0.5$ eV/atom. After deposition, the Al 2p feature (see inset) appears, indicating the successful deposition of Al.

1.6 Scanning tunneling microscopy

Within a small, transportable UHV chamber the sample can be transferred to another UHV chamber equipped with a STM. Magnetic transfer rods allow us to transport the sample towards the STM-part of the chamber, where a wobble stick is used to insert the sample into the STM. The STM is built up as a compact and mechanically stable construction [43]. For this purpose the coarse approach is formed by an inertial slider: the tip is mounted in a tiny tip holder, which is forced onto parallel tracks by a magnet. These tracks are glued to the front end of the piezo-tube, which is used for both driving the inertial slider and scanning the sample. In this way the mass of the moveable part is minimized, which leads to optimum mechanical stability.

As an example, Fig. 7 displays a comparison of two scanning tunneling microscope pictures: graphite surfaces

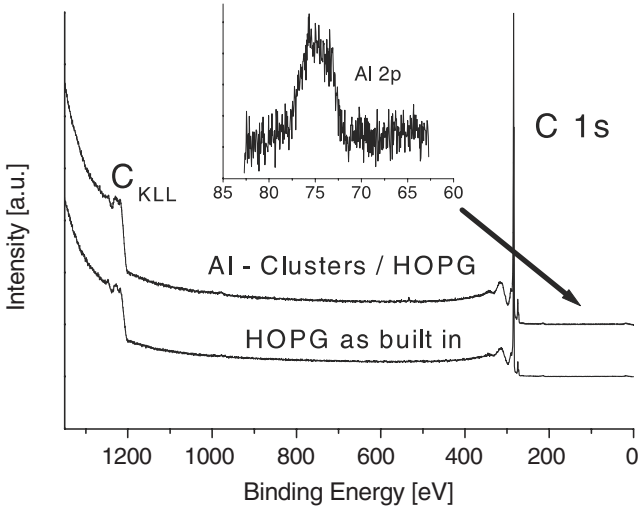

Fig. 6. Comparison of XPS spectra of a clean HOPG surface (*lower curve*) with a HOPG surface covered with 2% of an atomic monolayer of Al_n clusters with $n = 70 \pm 3$ (*upper curve*). The clusters have been deposited with a kinetic energy of 0.5 eV/atom

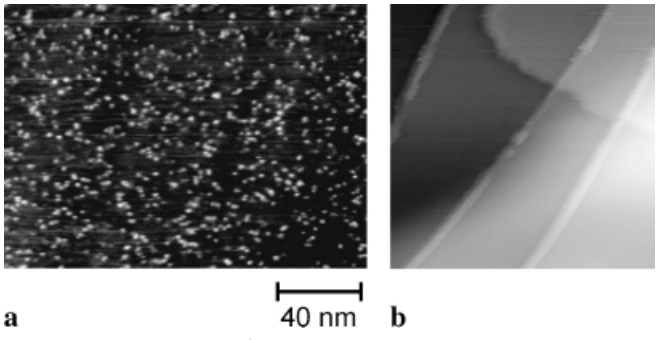

Fig. 7. a STM picture of Al^+ ions deposited on a HOPG surface with a kinetic energy of 10 eV. A considerable fraction of the ions created defects, which serve as nucleation sites for the deposited Al. Many relatively small Al particles pinned to such defect sites are observed at room temperature. The coverage is 4% of an atomic monolayer. **b** STM picture of a HOPG surface with Al_{70} clusters deposited at a kinetic energy of 10 eV corresponding to 0.14 eV/atom. The clusters are highly mobile on the surface and difficult to image with the STM. Therefore, the sample was moderately heated and the clusters condense at step edges. No surface defects are generated by the deposition process, indicating 'soft' landing. The coverage corresponds to 2% of an atomic monolayer. The scale is the same as in **a**

(HOPG) with (a) Al^+ ions and (b) Al_{70}^+ cluster ions deposited onto them with a kinetic energy of 10 eV. In Fig. 7a, some of the ions have created defects on the surface, which serve as nucleation sites and a relatively high density of small Al islands is observed. In contrast, Al_{70}^+ cluster ions deposited at the same kinetic energy are soft-landed and no defects are created in the HOPG surface. These clusters are highly mobile and difficult to observe using the STM, because the tip of the STM moves the clusters. Therefore, the sample has been heated slightly and the clusters nucleate at step edges as shown in Fig. 7b. Thus, the number of defects at the surface is low and the clusters are indeed soft-landed.

2 Deposition of 'magic' silicon clusters

If C_{60} clusters are deposited on an inert substrate like graphite (HOPG), the clusters are highly mobile at room temperature. Although clusters will 'collide' during their diffusion on the surface and although the total energy of a C_{120} cluster is larger than that of two C_{60} fullerenes, the C_{60} do not fuse to larger carbon particles. There is an activation barrier of this reaction, which is large compared to the thermal energy (at room temperature). This barrier enables C_{60} to be a building block for a cluster material.

We focus on the question of whether certain "magic" silicon clusters might posses similar properties. Recently, size-selected Si_{30}^+ and Si_{39}^+ cluster ions have been soft-landed on a Ag(111) surface, and at room temperature these clusters have been found to be mobile and they condense at step edges [44]. However, from this study it is not clear whether the clusters have merged to larger silicon particles or not. With the STM condensed material is detected at the edges with no further information about the detailed structure. Si_{30}^+ and Si_{39}^+ are not magic clusters, because they have relatively small HOMO-LUMO gaps (highest occupied molecular orbital, lowest unoccupied molecular orbital) [45]. A large gap (about 1 eV) indicates a magic cluster [46, 47]. Therefore, for our studies we selected Si_4 as a possible candidate as a building block for cluster material and deposited Si_4^- cluster anions on HOPG at a kinetic energy of 2 eV corresponding to 0.5 eV/atom. This cluster is known to be magic with a HOMO-LUMO gap comparable to C_{60} [45, 46].

Figure 8 displays a comparison of XPS spectra of the silicon $2p$ peak of Si_4 clusters (a) deposited on HOPG with that of bulk silicon (b). The coverage corresponds to 1% of a monolayer of Si atoms. The XPS spectrum of the clusters shows a certain contribution (10%) from Si–C. The appearance of reacted Si atoms can be explained by Si_4 clusters trapped at defect sites and step edges. Compared to bulk silicon, the main Si–Si peak exhibits a shift of 0.4 eV. Such a shift is typical for clusters with a lower average coordination number and is to be expected for individual clusters deposited on an inert surface. It is a (weak) hint that the tetramers might not have merged to larger islands. However, there are other possible explanations, like an interaction (e.g. charge transfer) with the surface.

Figure 9a displays a high-resolution STM picture of a single Si particle on the HOPG surface. This particle could be detected with the STM, because it did not move during the imaging process. It is pinned to a surface defect. To prove

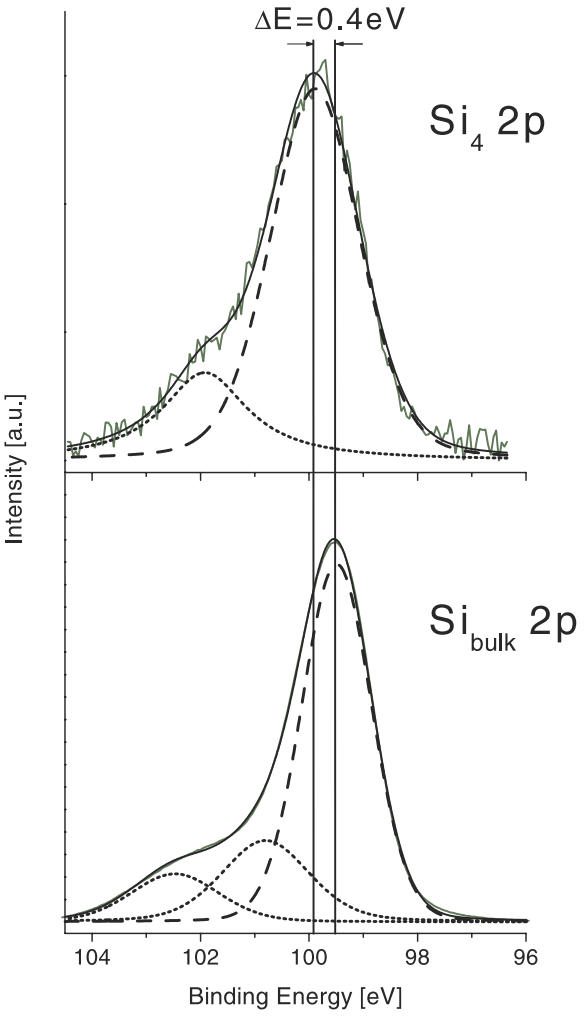

Fig. 8a,b. Comparison of XPS spectra of the silicon $2p$ peak for **a** Si_4 clusters deposited on HOPG and **b** bulk silicon. For the clusters, the coverage corresponds to 1% of a monolayer of Si atoms. The main peak at 100 eV corresponds to Si–Si bonds and the two peaks at higher binding energies are assigned to Si–C (101 eV) and Si–O (102.5 eV). For the upper curve, the appearance of the Si–C peak can be explained by Si_4 clusters trapped at surface defects (about 50% of the clusters). The Si–O peak is probably due to reactions with residual gas

this, the particle has been removed with the STM-tip and the same spot has been imaged again (Fig. 9b). Indeed, a surface defect (hole) is observed. The Si particle displayed in Fig. 9a has a size corresponding to roughly four Si_4 clusters.

It was not possible to observe mobile clusters, which are certainly there, because the coverage observed in the STM is lower than that detected with XPS. In Fig. 9c, a larger area of the sample is displayed and several agglomerations of Si trapped at defects are visible. In addition, some material is condensed at the step edge. However, where is the missing silicon? There is a feature in Fig. 9c, which hints to the existence of highly mobile material on the surface: the 'thread' in the left upper corner. Such threads indicate that the tip sweeps material during the scan and this material is highly mobile. However, using the STM we cannot gain any further information about these "free" clusters. Most likely, they form either a larger island consisting of amorphous silicon or an island consisting of weakly bound individual Si_4 clusters. In future studies, we will an-

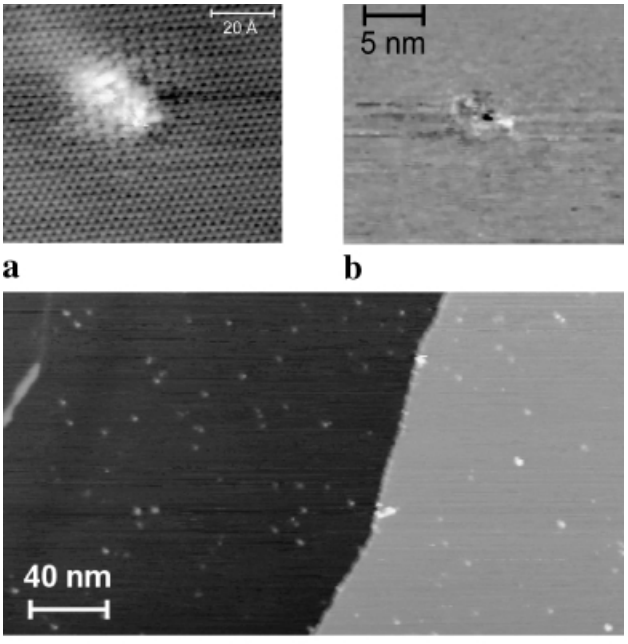

Fig. 9. a High-resolution STM image of a single Si particle trapped at a surface defect of graphite. The size of the particle corresponds to roughly four Si_4 clusters. **b** STM picture of the same spot as shown in **a** but with the silicon removed from the surface. The surface defect is visible as a dark spot. **c** STM picture of a larger area of the graphite surface decorated with 'soft-landed' Si_4 clusters. Most of the visible material (bright spots) are large Si islands trapped at surface defects and the step edge. In the left upper corner a "thread" is observed. Such a feature indicates the existence of highly mobile Si not visible using the STM

swer this question using HREELS (high-resolution electron energy loss spectroscopy) and UPS (ultraviolet photoelectron spectroscopy) to gain more information about the inner structure of the 'free' silicon islands and clusters on the surface.

3 Conclusion

We tested the suitability of a PACIS for cluster-deposition experiments and achieved cluster-ion currents of 3–6 nA for clusters with $n < 10$ atoms and of 0.5–1 nA for clusters with $n = 10$–100 atoms. The cluster ions are decelerated to kinetic energies far below the internal binding energy per atom in the clusters and the clusters are soft-landed on the substrate. The PACIS is suitable for the generation of clusters of various materials like Si, C, Ag, Cu, Pt, Au, Ti, S and P. In addition, clusters of compound materials like endohedral fullerenes and metallocarbohedrenes (metcars) can be effectively generated. The samples are studied using X-ray photoelectron spectroscopy and scanning tunneling microscopy.

First results on the deposition of magic Si_4 clusters on graphite at room temperature are discussed. Although there are some indications in the XPS and the scanning tunneling microscopy data supporting the assumption of individual clusters "surviving" at the surface, the formation of larger islands of bulk silicon by the fusion of clusters cannot be excluded. If these magic clusters do form islands of weakly interacting clusters analogous to C_{60}, new silicon-based cluster material could be synthesized. To answer this question the application of additional techniques like HREELS and UPS will be necessary.

References

1. W.A. de Heer: Rev. Mod. Phys. **65**, 611 (1993)
2. Z. Xu, F.-S. Xiao, S.K. Purnell, O. Alexeev, S. Kawi, S.E. Deutsch, B.C. Gates: Nature **372**, 346 (1994)
3. M.S. Dresselhaus, G. Dresselhaus, P.C. Eklund: *Science of Fullerenes and Carbon Nanotubes* (Academic, San Diego 1996)
4. S.B. DiCenzo, S.D. Berry, E.H. Hartford, Jr.: Phys. Rev. B **38**, 8465 (1988)
5. Y. Kuk, M.F. Jarrold, P.J. Silverman, J.E. Bower, W.L. Brown: Phys. Rev. B **39**, 11 168 (1989)
6. P. Fayet, F. Granzer, G. Hegenbart, E. Moisar, B. Pischel, L. Wöste: Phys. Rev. Lett. **55**, 3002 (1985)
7. W. Eberhardt, P. Fayet, D.M. Cox, Z. Fu, A. Kaldor, R. Sherwood, D. Sondericker: Phys. Rev. Lett. **64**, 780 (1990)
8. G. Vandoni, C. Felix, R. Monot, J. Buttet, W. Harbich: Chem. Phys. Lett. **229**, 51 (1994)
9. K. Bromann, C. Felix, H. Brune, W. Harbich, R. Monot, J. Buttet, K. Kern: Science **274**, 956 (1996)
10. K. Bromann, H. Brune, C. Felix, W. Harbich, R. Monot, J. Buttet, K. Kern: Surf. Sci. **377**, 1051 (1997)
11. H.-V. Roy, J. Boschung, P. Fayet, F. Patthey, W.-D. Schneider: Z. Phys. D **26**, 252 (1993)
12. H.-V. Roy, P. Fayet, F. Patthey, W.-D. Schneider, B. Delley, C. Massobrio: Phys. Rev. B **49**, 5611 (1994)
13. U. Busolt, E. Cottancin, H. Röhr, L. Socaciu, T. Leisner, L. Wöste: Appl. Phys. B **68**, 453 (1999)
14. W. Yamaguchi, K. Yoshimura, Y. Maruyama, K. Igarashi, S. Tanemura, J. Murakami: Chem. Phys. Lett. **311**, 341 (1999)
15. W. Yamaguchi, K. Yoshimura, Y. Maruyama, K. Igarashi, S. Tanemura, J. Murakami: Chem. Phys. Lett. **311**, 415 (1999)
16. G.M. Francis, I.M. Goldby, L. Kuipers, B. von Issendorff, R.E. Palmer: J. Chem. Soc., Dalton Trans. **1996**, 665 (1996)
17. S.G. Hall, M.B. Nielsen, R.E. Palmer: J. Appl. Phys. **83**, 733 (1998)
18. S.J. Carroll, S.G. Hall, R.E. Palmer: Phys. Rev. Lett. **81**, 3715 (1998)
19. C.-M. Grimaud, L. Siller, M. Andersson, R.E. Palmer: Phys. Rev. B **59**, 9874 (1999)
20. S.J. Carroll, P. Weibel, B. von Issendorff, L. Kuipers, R.E. Palmer: J. Phys.: Condens. Matter **8**, L617 (1996)
21. S.J. Carroll, R.E. Palmer, P.A. Mulheran, S. Hobday, R. Smith: Appl. Phys. A **67**, 613 (1998)
22. S.J. Carroll, K. Seeger, R.E. Palmer: Appl. Phys. Lett. **72**, 305 (1998)
23. U. Heiz: Appl. Phys. A **67**, 621 (1998)
24. U. Heiz, F. Vanolli, A. Sanchez, W.-D. Schneider: J. Am. Chem. Soc. **120**, 9668 (1998)
25. U. Heiz, A. Sanchez, S. Abbet, W.-D. Schneider: J. Am. Chem. Soc. **121**, 3214 (1999)
26. G. Ganteför, H.R. Siekmann, H.O. Lutz, K.H. Meiwes-Broer: Chem. Phys. Lett. **165**, 293 (1990)
27. H.R. Siekmann, Ch. Lüders, J. Fährmann, H.O. Lutz, K.H. Meiwes-Broer: Z. Phys. D **20**, 417 (1991)
28. Chia-Yen Cha, G. Ganteför, W. Eberhardt: Rev. Sci. Instrum. **63**, 5661 (1992)
29. Bu. Wrenger, K.H. Meiwes-Broer: Rev. Sci. Instrum. **68**, 2027 (1997)
30. K. Sattler, J. Mühlbach, A. Reyes-Flotte, E. Recknagel: Adv. Mass Spectrosc. **8**, 1826 (1980)
31. O.F. Hagena: Z. Phys. D **17**, 157 (1990)
32. I.M. Goldby, B. von Issendorff, L. Kuipers, R.E. Palmer: Rev. Sci. Instrum. **68**, 3327 (1997)
33. S.G. Hall, M.B. Nielson, A.W. Robinson, R.E. Palmer: Rev. Sci. Instrum. **68**, 3335 (1997)
34. V.E. Bondybey, J.E. English: J. Chem. Phys. **74**, 6978 (1981)
35. T.G. Dietz, M.A. Duncan, D.E. Powers, R.E. Smalley: J. Chem. Phys. **74**, 6511 (1981)
36. U. Heiz, F. Vanolli, L. Trento, W.D. Schneider: Rev. Sci. Instrum. **68**, 1986 (1997)

37. H. Handschuh, Chia-Yen Cha, H. Möller, P.S. Bechthold, G. Ganteför, W. Eberhardt: Chem. Phys. Lett. **227**, 496 (1994)
38. H. Handschuh, G. Ganteför, B. Kessler, P.S. Bechthold, W. Eberhardt: Phys. Rev. Lett. **74**, 1095 (1995)
39. G. Ganteför, M. Maus, W. Eberhardt: Appl. Phys. A **70**, 535 (2000)
40. H.R. Siekmann, E. Holub-Krappe, Bu. Wenger, Ch. Pettenkofer, K.H. Meiwes-Broer: Z. Phys. B **90**, 201 (1993)
41. G. Ganteför, S. Hunsicker, R.O. Jones: Chem. Phys. Lett. **236**, 43 (1995)
42. R.O. Jones, G. Ganteför, S. Hunsiker, P. Pieperhoff: J. Chem. Phys. **103**, 9549 (1995)
43. F. Mugele, A. Rettenberger, J. Boneberg, P. Leiderer: Rev. Sci. Instrum. **69**, 1765 (1998)
44. S. Messerli, S. Schintke, K. Morgenstern, A. Sanchez, U. Heiz, W.-D. Schneider: Surf. Sci. **465**, 331 (2000)
45. J. Müller, B. Liu, A.A. Shvartsburg, S. Ogut, J.R. Chelikowsky, K.W.M. Siu, K.-M. Ho, G. Ganteför: Phys. Rev. Lett. **85**, 1666 (2000)
46. H. Kietzmann, R. Rochow, G. Ganteför, W. Eberhardt, K. Vietze, W. Eberhardt, P.W. Fowler: Phys. Rev. Lett. **81**, 5378 (1998)
47. B.K. Rao, P. Jena, S. Burkart, G. Ganteför, G. Seifert: Phys. Rev. Lett. **86**, 692 (2001)